Research Square

Preprints are preliminary reports that have not undergone peer review.
They should not be considered conclusive, used to inform clinical practice,
or referenced by the media as validated information.

Assessing network RTK degradation under ionospheric disturbances using the I95 index

Luyang Zhang
Shandong Normal University (SDNU)
Bingcheng Liu
liubc@aircas.ac.cn
Aerospace Information Research Institute, Chinese Academy of Sciences
Ningbo Wang
Aerospace Information Research Institute, Chinese Academy of Sciences
Zishen Li
Aerospace Information Research Institute, Chinese Academy of Sciences
Chenxu Wang
Qilu Aerospace Information Research Institute (Shandong Laboratory of Aerospace Information Research at Jinan)
Mengfei Sun
Aerospace Information Technology University (AITech)
Zhenyao Liu
Aerospace Information Research Institute, Chinese Academy of Sciences
Zhiyu Wang
Aerospace Information Research Institute, Chinese Academy of Sciences

Research Article

Keywords: I95 index, Network RTK, ionospheric disturbances, Double-differenced ionospheric residuals, Ambiguity resolution, Quantile regression

Posted Date: July 29th, 2026

DOI: https://doi.org/10.21203/rs.3.rs-10409869/v1

License: This work is licensed under a Creative Commons Attribution 4.0 International License.
Read Full License

Additional Declarations: No competing interests reported.

Assessing network RTK degradation under ionospheric disturbances using the I95 index

Luyang Zhang[1,2,4], Bingcheng Liu[3,4*], Ningbo Wang[3], Zishen Li[3,4], Chenxu Wang[4], Mengfei Sun[2], Zhenyao Liu[3], Zhiyu Wang[3]

[1] School of Computer Science and Artificial Intelligence, Computer Science and Technology, Shandong Normal University (SDNU), 250358 Jinan, China

[2] Aerospace Information Technology University (AITech), 250200 Jinan, China

[3] Aerospace Information Research Institute, Chinese Academy of Sciences, Beijing, 100094, China

[4] Qilu Aerospace Information Research Institute (Shandong Laboratory of Aerospace Information Research at Jinan), Jinan 250100, China

Corresponding author: Bingcheng Liu (liubc@aircas.ac.cn)

Abstract

Ionospheric disturbances significantly affect the performance of network RTK (NRTK), particularly at low latitudes where ionospheric gradients may vary rapidly across regional reference networks. This study evaluates the use of the I95 index, derived from double-differenced ionospheric residuals, as an empirical indicator of NRTK performance degradation. Full-year GPS data from a 13-station CORS network in Hong Kong for 2019 and 2024 were processed using a leave-one-out virtual reference station (VRS) processing strategy. The relation between I95 and NRTK performance was assessed by the quantile regression. The results reveal a systematic degradation of NRTK performance with increasing I95, characterized by lower ambiguity-fixing rates, broader positioning error distributions, and increased sensitivity of the upper error quantiles. These effects were markedly stronger in 2024 than in 2019. For the 2024 dataset, the probability of 3D-RMS errors exceeding 10 cm increased from 11.3% for I95 values of 0–1 ppm to 88.5% for values above 20 ppm. Over the same range, the mean cumulative positioning error increased from 0.07 to 1.56cm/km, corresponding to a factor of about 22. The fitted exceedance model yielded probability levels of 40%, 60% and 80% at I95 values of approximately 4.16, 8.28 and 14.83 ppm, respectively. Based on the combined exceedance and cumulative-error characteristics, four empirical performance regimes were defined for the Hong Kong network, with I95 intervals of <4, 4–10, 10–16 and >16 ppm. The 2019 results preserved the general ordering of these regimes but exhibited a weaker response and limited sampling at high I95 values. The derived thresholds provide a practical regional link between residual

ionospheric monitoring and user-domain NRTK performance under low-latitude conditions.

Keywords

I95 index; Network RTK; ionospheric disturbances; Double-differenced ionospheric residuals; Ambiguity resolution; Quantile regression

Introduction

Network real-time kinematic (NRTK) positioning, based on Global Navigation Satellite Systems (GNSS), provides centimeter-level accuracy and supports applications such as surveying, exploration, and intelligent driving (Naciri et al. 2023). NRTK performance depends on the capability of the reference network to model and interpolate distance-dependent errors. Residual ionospheric delays are often the dominant limitation over short to medium baselines, particularly in low-latitude regions where ionospheric gradients can vary rapidly (Lyu et al. 2025; Wang et al. 2026). During the high-activity phase of solar cycle 25, increased ionospheric scintillation and rapid variations in total electron content (TEC) can degrade observation quality (Li et al. 2020; Li et al. 2026), reduce ambiguity-fixing reliability, and affect the continuity of NRTK services (Zhang W et al. 2025). For operational NRTK services, it is therefore essential to quantify how ionospheric residuals observed within the reference network translate into degraded user-side ambiguity resolution and positioning performance.

Previous studies have demonstrated the adverse impact of ionospheric disturbances on NRTK positioning. However, the residual-error pathway within the NRTK processing chain has not yet been quantified in a systematic way. In particular, the role of double-differenced (DD) ionospheric residuals in ambiguity resolution and user-side positioning degradation remains insufficiently characterized under disturbed conditions (Guerra et al. 2024). This limits both the attribution of positioning errors to imperfect network interpolation and the definition of operationally meaningful warning levels. Ionospheric disturbance indices such as the Rate of TEC Index (ROTI, Zhang Z et al. 2025) and the Gradient Ionosphere index (GIX, Nykiel et al. 2024) are commonly derived from GNSS TEC observations and describe ionospheric variability at different spatial and temporal scales. They are, however, not defined in the same DD residual domain as NRTK interpolation errors. The DD ionospheric residuals represent the ionospheric error components that remain after network modeling and interpolation, and are therefore more directly linked to ambiguity-fixing reliability and user-side positioning accuracy (Weaver 2023). The residual-based indicators can thus provide a closer connection to NRTK service monitoring than TEC-based indices alone.

Wanninger (1999) introduced the I95 index as a network-level measure of ionospheric disturbance for NRTK applications. The index is derived from DD ionospheric residuals within the

reference network and is commonly expressed as an hourly 95th percentile normalized by baseline length. In this form, I95 provides a compact description of the residual ionospheric activity in the same error domain as NRTK interpolation. Chen et al. (2003) later introduced ionospheric residual integrity monitoring (IRIM) and ionospheric residual interpolation uncertainty (IRIU) to assess ionospheric interpolation quality and user-side uncertainty. Compared with these approaches, I95 is simpler to compute and does not require station removal or a predefined user position. It is therefore well suited for continuous network monitoring and for empirical studies relating ionospheric residual activity to user-side NRTK performance.

Although I95-based studies have provided useful evidence for NRTK service monitoring, the relation between I95 and user-side performance remains only partly quantified. Earlier work suggested that I95 values above about 4 ppm may increase the risk of initialization problems (Wanninger 2004). The associated changes in ambiguity-fixing rate, positioning error, and large-error probability have not been assessed systematically over a wide range of disturbance levels. Existing thresholds are therefore mainly empirical and remain only weakly supported by user-domain positioning statistics (Gianniou et al. 2012; Próchniewicz et al. 2017). For operational services, this uncertainty may result either in overly conservative warnings and reduced availability or in delayed recognition of degraded positioning reliability (Paziewski 2016; Li et al. 2025). This is particularly relevant during periods of enhanced solar activity, when strong spatial ionospheric gradients and rapid temporal variations are more likely to compromise network interpolation performance.

This study assesses I95 as a network-internal indicator of user-side NRTK degradation in a low-latitude regional network. Full-year observations from the Hong Kong CORS network in 2019 and 2024 are processed in a leave-one-out virtual reference station (VRS) configuration to relate network-level DD ionospheric residuals to NRTK ambiguity resolution and positioning performance. The analysis first examines the dependence of ambiguity-fixing rate and 3D positioning error on I95, and then uses year-specific quantile regression to assess whether this dependence is enhanced in the upper tail of the error distribution. Exceedance probabilities for 3D positioning errors above 10 cm and cumulative positioning errors per baseline length are combined to derive network-specific I95 intervals for the Hong Kong case study. The results show how a network-level DD ionospheric residual indicator can be linked to user-domain NRTK degradation under disturbed ionospheric conditions. The paper is organized as follows. The analysis method and data processing strategy are first described, followed by the assessment of I95-dependent NRTK performance in the Hong Kong low-latitude network. The final section summarizes the main conclusions and limitations.

Methods

This section describes the processing and analysis strategy used to relate I95 to user-side NRTK

performance. The VRS experiment is introduced first, followed by the estimation of DD ionospheric residuals and the computation of hourly I95 values. The dataset, processing settings, and statistical analysis are then presented as the basis for the subsequent performance assessment.

NRTK processing

The NRTK analysis employs a leave-one-out VRS strategy. For each test, one station of the Hong Kong CORS network is excluded from the reference-network solution and treated as an independent user station. The remaining stations are used for server-side network estimation and for generating VRS observations at or in the immediate vicinity of the excluded station. This separation enables network-derived ionospheric residuals to be related to user-side ambiguity resolution and positioning performance, without involving observations from the test station in the corresponding network solution.

The processing chain consists of three steps. First, DD baseline solutions are formed between the reference stations, and residual atmospheric delays are estimated after ambiguity fixing. Second, the estimated ionospheric and tropospheric residuals are interpolated to the VRS location using the adopted interpolation model. Finally, user-side RTK positioning is performed between the generated VRS observations and the observations of the excluded station. The first two steps constitute the server-side NRTK processing, while the final step provides the independent user-side performance assessment.

For a reference-network baseline, the DD carrier-phase and pseudorange observation equations can be written as

$$\begin{cases} \Delta\nabla\phi_{k,s}^{i,j} = \Delta\nabla\rho_{k,s}^{i,j} + \lambda_s\Delta\nabla N_{k,s}^{i,j} - \Delta\nabla I_{k,s}^{i,j} + \Delta\nabla T_{k,s}^{i,j} + \varepsilon \\ \Delta\nabla P_{k,s}^{i,j} = \Delta\nabla\rho_{k,s}^{i,j} + \Delta\nabla I_{k,s}^{i,j} + \Delta\nabla T_{k,s}^{i,j} + \varepsilon \end{cases} \tag{1}$$

where $\Delta\nabla$ denotes the DD operator, superscripts i and j denote satellites, subscript k denotes the reference station, and subscript s denotes the frequency. ϕ is the carrier-phase observable, P is the pseudorange observable, ρ is the geometric range, λ is the wavelength of frequency, N is the integer ambiguity, I is the first-order ionospheric delay term, T is the tropospheric delay term, and ε is the observation noise.

Following successful DD ambiguity fixing, the residual atmospheric delays are estimated for the reference-network baselines. These estimates are subsequently interpolated to the VRS location and applied in generating the VRS observations (Gao et al. 2025; Liu et al. 2026). The user-side DD observation model between the VRS (V) and the excluded user station (U) can then be expressed as

$$\begin{cases} \Delta\nabla\phi_{V,U,s}^{i,j} = \Delta\nabla\rho_{V,U}^{i,j} + \lambda_s\Delta\nabla N_{V,U,s}^{i,j} - \delta I_{V,U,s}^{i,j} + \delta T_{V,U}^{i,j} + \varepsilon \\ \Delta\nabla P_{V,U,s}^{i,j} = \Delta\nabla\rho_{V,U}^{i,j} + \delta I_{V,U,s}^{i,j} + \delta T_{V,U}^{i,j} + \varepsilon \end{cases} \tag{2}$$

Here, δI and δT denote the residual DD ionospheric and tropospheric delays remaining after applying network corrections, respectively. Under nominal ionospheric conditions, these distance-dependent residuals are expected to be small because the VRS is generated in close proximity to the user station. During disturbed periods, however, the spatial variability of the ionosphere may not be fully represented by the interpolation model. The resulting residual ionospheric delays in Eq. (2) may reduce ambiguity-fixing reliability and degrade the positioning solution.

The residual ionospheric term in the user-side model is related to the residual ionospheric activity observed within the reference network. The I95 index, however, is neither applied as a correction nor introduced as a constraint in the positioning filter. Instead, it is derived independently from DD ionospheric residuals of the reference-network solutions and used only as an explanatory indicator in the subsequent performance analysis. This study therefore evaluates the diagnostic value of I95 for identifying NRTK performance degradation, rather than an I95-based correction or mitigation strategy.**Extraction of DD ionospheric residuals for I95 computation**

During periods of enhanced ionospheric activity, DD ionospheric residuals constitute one of the principal error sources in NRTK positioning. Their extraction is based on the DD carrier-phase model:

$$\Delta\nabla\phi_{k,s}^{i,j} = \Delta\nabla\rho_{k,s}^{i,j} + \lambda_s\Delta\nabla N_{k,s}^{i,j} - \Delta\nabla I_{k,s}^{i,j} + \Delta\nabla T_{k,s}^{i,j} + \varepsilon \tag{3}$$

where the notation follows that introduced for Eq. (1).

After wide-lane ambiguity resolution using the MW combination and integer ambiguity fixing within the reference network, the remaining unknown terms are the DD tropospheric and ionospheric residuals. Using the non-dispersive property of tropospheric delay, the ionosphere-free combination is formed on the L1 frequency to estimate the DD tropospheric residual

$$\Delta\nabla T = \frac{{f_1}^2}{{f_1}^2-{f_2}^2}\lambda_1(\Delta\nabla\phi_1 - \Delta\nabla N_1) - \frac{{f_2}^2}{{f_1}^2-{f_2}^2}\lambda_2(\Delta\nabla\phi_2 - \Delta\nabla N_2) - \Delta\nabla\rho \tag{4}$$

where f_1 and f_2 are the carrier frequencies, $\Delta\nabla\phi$ is the DD carrier-phase observable, $\Delta\nabla N$ denotes the DD ambiguity, and $\Delta\nabla T$ denotes the DD tropospheric residual. Once the DD tropospheric residual $\Delta\nabla T$ is determined, the DD ionospheric residual can be obtained from the ambiguity-fixed L1 carrier-phase residual as

$$\Delta\nabla I_{k,s}^{i,j} = \Delta\nabla\rho_{k,s}^{i,j} + \lambda_s\Delta\nabla N_{k,s}^{i,j} - \Delta\nabla\phi_{k,s}^{i,j} + \Delta\nabla T_{k,s}^{i,j} + \varepsilon \tag{5}$$

where $\Delta\nabla I$ is the estimated L1 DD ionospheric residual, and $\Delta\nabla T$ is the estimated DD tropospheric residual.

In the present analysis, the extracted DD ionospheric residuals are used only to compute the I95 index as an indicator of regional ionospheric disturbance activity. This index is neither estimated as a state parameter in the user-side filter nor applied in generating the VRS observations. In the I95 computation, the carrier-phase noise and remaining unmodeled phase errors are not estimated separately. Instead, after ambiguity fixing and removing the estimated tropospheric contribution, the residual term $\Delta\nabla I$ is treated as the DD ionospheric residual for I95 computation.

The master station and the set of effective baselines are selected according to data availability, observation quality, dilution of precision, the number and elevation of commonly tracked satellites, and observation continuity. As a result, the set of valid baselines and DD residual samples may vary with time. The extracted DD ionospheric residuals reflect both the prevailing ionospheric conditions and the instantaneous network geometry. To provide a compact network-level description, the residuals are normalized by their respective baseline lengths and summarized by the hourly I95 statistic.

I95 index computation and normalization

The I95 index condenses DD ionospheric residuals observed across the reference network into a single measure of regional residual ionospheric activity (Wanninger 1999). It is defined as the 95% quantile of all DD ionospheric residuals within a predefined time window, typically 1 h, and can be written as follows:

$$\begin{cases} I_n = \sum_{n=1}^{k*s} \sqrt{I_{LAT,n}^2 + I_{LON,n}^2} = \sqrt{\sum_{n=1}^{k*s} \Delta\nabla I^2} \\ I_{95}: P(I_n < I_{95}) = 95\%, P(I_n > I_{95}) = 5\% \end{cases} \quad (6)$$

where I_n denotes the ionospheric residual magnitude sample in every epoch used for the I95 computation, and its latitudinal and longitudinal components are denoted by I_{LAT} and I_{LON} I_{LON}, respectively. In the present implementation, the DD ionospheric residual $\Delta\nabla I$ derived from the ambiguity-fixed observations is used directly. Here, the index *n* denotes the residual-sample number, *k* is the number of valid baselines, *s* is the number of valid DD residuals, or satellite pairs, for each baseline at a given epoch, and *k*s* is the total number of valid samples used for I95 computation within the corresponding hourly interval.

On the server side, I95 is computed from DD ionospheric residuals accumulated over successive 1h intervals. As a baseline-normalized error measure, it is expressed in parts per million (ppm), with 1 ppm corresponding to mm/km. For each valid baseline and epoch, the absolute residual is normalized by the baseline length. All normalized samples from the reference network are

subsequently pooled within the corresponding hourly interval, and their empirical 95th percentile is adopted as the I95 value. The resulting index is used exclusively as an external explanatory indicator in the performance assessment and is not introduced into the user-side positioning filter.

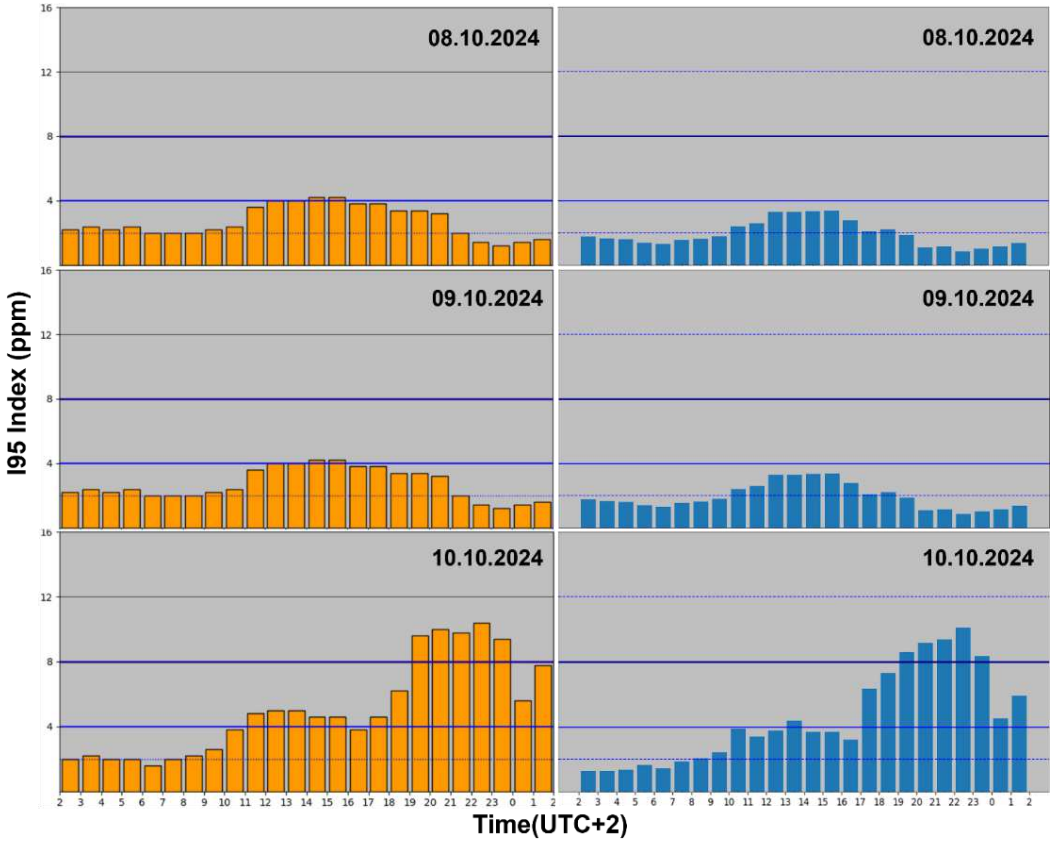


Fig. 1 Comparison of hourly I95 values from the operational LGLN product (left column) and the series computed in this study (right column) for Germany during 8-10 October 2024. I95 is expressed in ppm, equivalent to mm/km after normalization by baseline length.

As an external consistency check, the hourly I95 series derived in this study from a selected set of German reference stations was compared with the real-time I95 product provided by LGLN (https://i95.sapos.de) for 8-10 October 2024, as shown in Fig. 1. Both I95 series exhibit consistent temporal variations and comparable magnitudes, with differences generally below 1 ppm. The remaining discrepancies can be attributed to differences in station selection and processing mode, since the present I95 values were derived from post-processed data and a specific station selection, whereas the LGLN product is generated operationally in real time. The close agreement supports the consistency of the implemented I95 computation and its ability to characterize the regional residual ionospheric activity.

Quantile regression analysis

Quantile regression is used to assess the dependence of NRTK positioning errors on I95 across different parts of the error distribution. This is of particular relevance because ionospheric disturbances may affect not only the mean or median positioning error, but also the upper tail associated with large-error events. In contrast to ordinary least-squares regression, which describes the conditional mean, quantile regression estimates selected conditional quantiles and thus allows separate assessment of the low-, median-, and high-error regimes.

For a given quantile level $\tau \in (0, 1)$, the conditional quantile model is written as

$$Q_Y(\tau \mid X) = X^T\beta(\tau) \tag{7}$$

where $Q_Y(\tau \mid X)$ denotes the conditional τ-quantile of the dependent variable Y given the covariates X. The parameter vector is obtained by minimizing the weighted sum of absolute residuals

$$\hat{\beta}(\tau) = argmin_\beta \sum_{i=1}^{n} \rho_\tau (Y - X^T\beta) \tag{8}$$

where $\rho\tau(u) = u\big(\tau - I(u < 0)\big)$ is the check function and $I(\cdot)$ is the indicator function.

Separate quantile regression models are fitted to 2019 and 2024 datasets to characterize the dependence of NRTK positioning errors on I95 under different ionospheric conditions. For each quantile level τ, the conditional quantile of 3D-RMS error is expressed as a function of I95, with the fitted slope providing a measure of the corresponding error sensitivity. Comparison of the slopes across quantiles and between years allows the I95 response to be assessed throughout the error distribution and under comparatively quiet and active ionospheric conditions.

Datasets and processing

The analysis is based on GPS observations from 13 stations of the Hong Kong CORS network, with inter-station distances of less than 30 km (https://www.geodetic.gov.hk). Owing to its low-latitude location and pronounced ionospheric variability, the network provides a suitable test environment for assessing ionospheric effects on NRTK performance. The station distribution is shown in Fig. 2, where the green markers denote reference stations and the red dot indicates the VRS location for the illustrated test configuration. A leave-one-out strategy is adopted for the NRTK experiments. Full-year datasets from 2019 and 2024 are considered to represent periods of comparatively low and high solar and ionospheric activity, respectively.

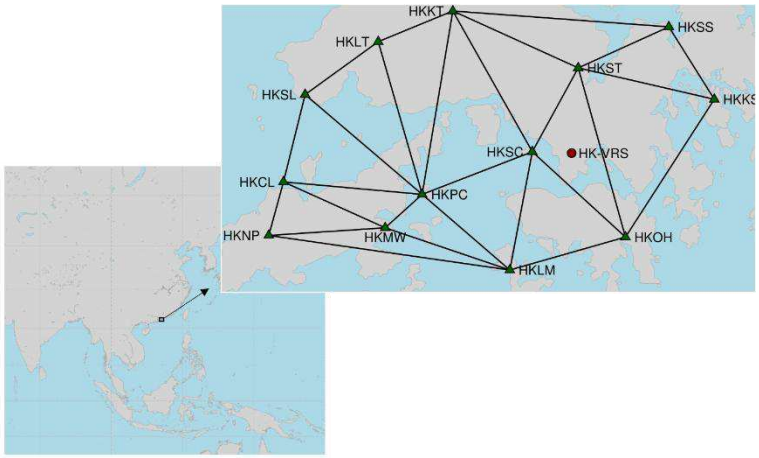


Fig. 2 Geographic distribution of the Hong Kong CORS network. Green triangles denote the reference stations, and the red circle denotes the VRS location.

Table 1 Processing settings for server-side network estimation and user-side VRS positioning.

Item	Strategy	
	Server-side processing	User-side processing
Station coordinates	Hong Kong Satellite Positioning Reference Station Network (https://www.geodetic.gov.hk/common/data/pdf/SatRef_Coord.pdf)	
GNSS observations	GPS L1/L2 observations	
Sampling interval	30s	
Priori observation noise	Pseudorange: 0.3 m, carrier-phase: 0.003 m	
Combination mode	Ionosphere-free combination	
Cut-off elevation	15°	10°
Weighting strategy	Elevation & SNR-dependent weighting	Elevation-dependent weighting
Carrier-phase ambiguity	WL-L1 cascade fixing with constants for each continuous observation arc	L1/L2 partial ambiguity fixing; ambiguity held constants over each continuous tracking arc
Ionospheric delay	First-order contribution eliminated, higher order terms neglected	Corrected using a linear interpolation model (LIM)
Tropospheric delay	Dry Component: modeled by Saastamoinen with NMF Wet Component: estimated as an hourly constant with process noise of 1 cm/$\sqrt{h}$ and NMF	Corrected using a LIM

Carrier-phase ambiguities are resolved using the least-squares ambiguity decorrelation adjustment method (LAMBDA, Teunissen 1995). The reliability of ambiguity resolution is assessed by means of the ratio test, which compares the ambiguity residuals associated with the best and second-best integer candidates (Teunissen et al. 2004). A solution is accepted as fixed when the LAMBDA search is successful and the ratio exceeds the adopted threshold of 3.0. The detailed server- and user-side processing settings are summarized in Table 1.

On the server side, dual-frequency observations from the Hong Kong Satellite Positioning

Reference Station Network are processed at a sampling rate of 30s, with the published station coordinates held fixed. The ionosphere-free combination is formed to eliminate the first-order ionospheric delay, while higher-order ionospheric effects are neglected. The dry tropospheric component is modeled using the Saastamoinen model together with the Niell Mapping Function (NMF, Niell., 1996), whereas the wet component is estimated as an hourly constant with a process noise of $1\text{cm}/\sqrt{h}$. An elevation cut-off angle of 15° is applied, and the stochastic model is defined as a function of both satellite elevation and signal-to-noise ratio (SNR). Carrier-phase ambiguities are resolved using WL/L1 cascade strategy and are maintained as constants within each continuous observation arc.

User-side positioning is performed in the VRS mode using the same dual-frequency observations and sampling interval. An elevation cut-off angle of 10° is adopted together with an elevation-dependent weighting stochastic model. The residual ionospheric and tropospheric delays are corrected using the linear interpolation model derived from the reference network. The L1 and L2 ambiguities are processed using partial ambiguity fixing, and are retained as constants within each continuous observation arc.

Results and discussion

This section evaluates the dependence of NRTK performance on I95 for the low-latitude Hong Kong network. The temporal variations in positioning error, ambiguity-fixing rate, and hourly I95 are compared for 2019 and 2024. The I95-dependent changes in ambiguity resolution, 3D-RMS error, and conditional error quantiles are then examined. Finally, exceedance probabilities and cumulative-error statistics are combined to derive empirical regional risk intervals.

Relationship between I95 and NRTK performance

The relationship between I95 and NRTK performance is first examined using the horizontal positioning errors obtained from the leave-one-out solutions. Fig. 3 presents the epoch-wise horizontal positioning errors for 2019 and 2024. In 2019, the errors are concentrated close to the coordinate origin, with most solutions remaining at the cm level and only a limited high-error tail. In 2024, the error distribution is markedly broader and contains a substantially larger fraction of high-error samples. The enhanced ionospheric activity in 2024 was accompanied by both increased positioning errors and reduced solution stability.

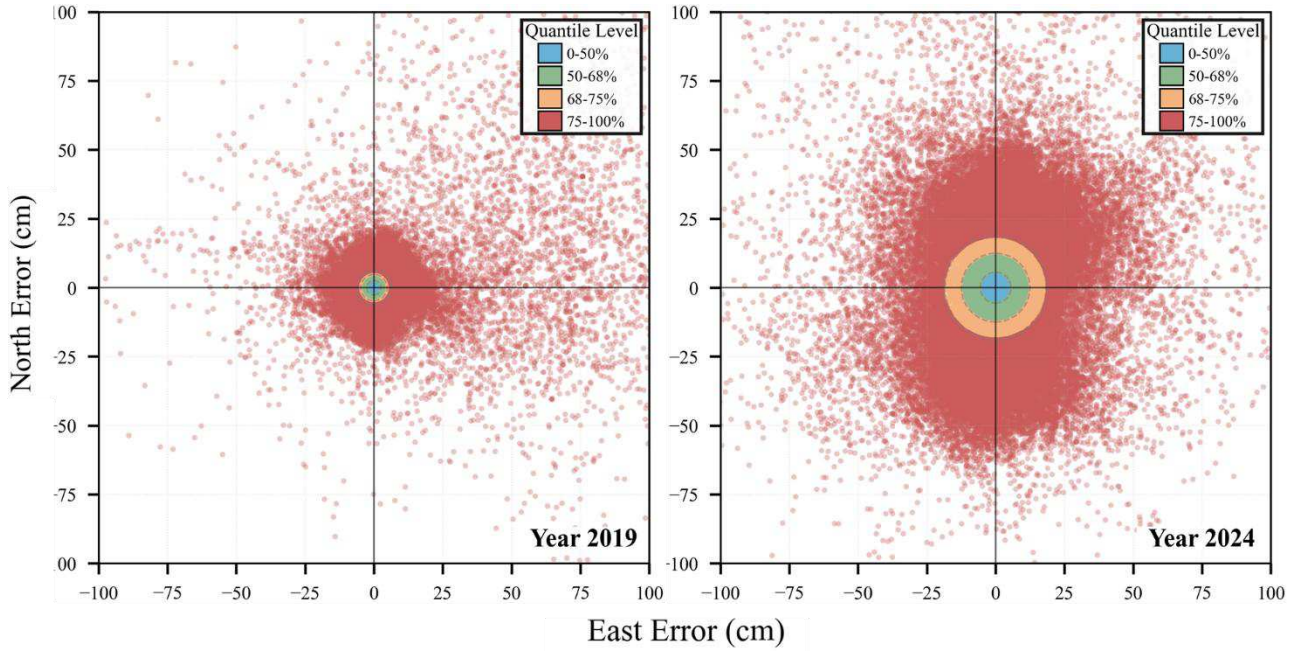


Fig. 3 Horizontal positioning errors of the NRTK solutions for 2019 and 2024. Individual points represent epoch-wise east and north errors, while the colored circles indicate selected quantiles of the radial positioning error.

Fig. 4 shows the user-side ambiguity-fixing rate as a function of day of year (DOY) and UTC hour. The fixing rate exceeds 90% for approximately 87.8% of the hourly bins in 2019, compared with only 53.1% in 2024. The 2024 results exhibit extended periods of reduced fixing performance, particularly around 12:00 UTC.

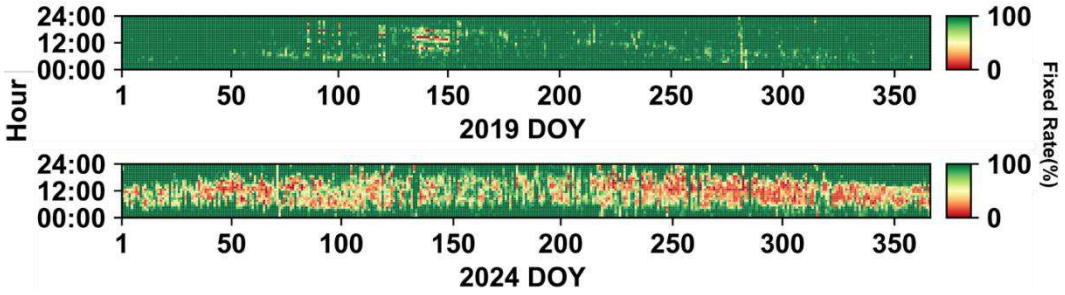


Fig. 4 Temporal variation of the user-side NRTK ambiguity-fixing rate for the Hong Kong CORS network in 2019 and 2024. Values are shown as a function of DOY and UTC hour.

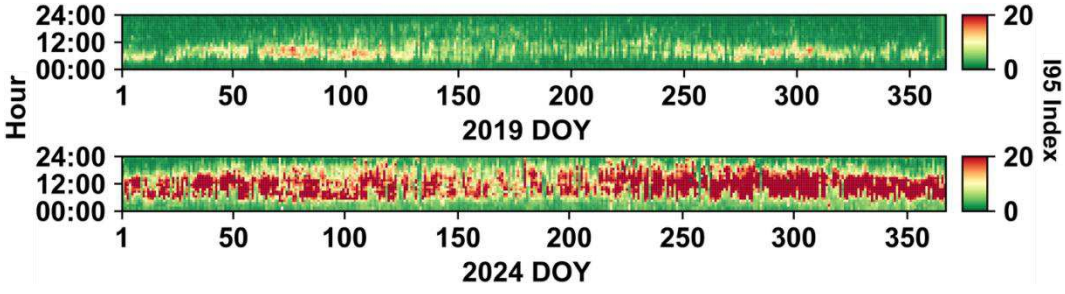


Fig. 5 Temporal variation of hourly I95 values for the Hong Kong CORS network in 2019 and 2024.

The hourly I95 values in Fig. 5 provide the ionospheric context for the ambiguity-fixing pattern shown in Fig. 4. I95 remains mostly below 2 ppm in 2019, consistent with generally high fixing rates. In contrast, elevated I95 values occur much more frequently in 2024 and are concentrated around 12:00 UTC, where they broadly coincide with reduced ambiguity-fixing performance. This time corresponds to approximately 20:00 local time in Hong Kong, when post-sunset ionospheric irregularities associated with the pre-reversal enhancement may become more pronounced at low latitudes. Since VRS positioning relies on spatially interpolated atmospheric corrections, enhanced ionospheric variability during these periods may degrade the correction quality and reduce ambiguity-resolution reliability.

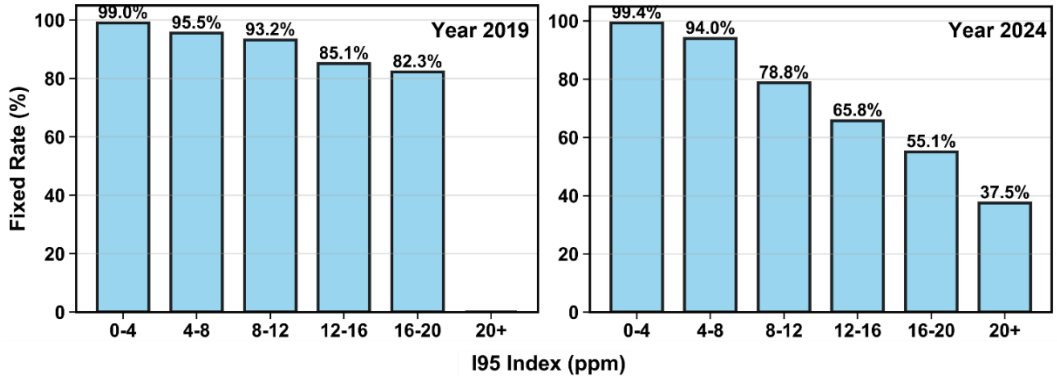


Fig. 6 User-side NRTK ambiguity-fixing rate for different I95 intervals in 2019 and 2024.

For the interval-based analysis shown in Figs. 6 and 7, the I95 values are grouped into bins of 4 ppm. This bin width provides a balance between resolving I95-dependent performance changes and retaining sufficient samples within each interval. It is also consistent with the 4 ppm reference level commonly adopted in previous I95-based NRTK studies (Wanninger 2004).

Fig. 6 shows the ambiguity-fixing rate for the individual I95 intervals. In 2019, the fixing rate decreases gradually with increasing I95, but remains above 82% over the 0–20 ppm range, with no samples in the above 20 ppm interval. In 2024, the degradation is more pronounced. The fixing rate is 99.4% in the 0–4 ppm interval, close to the 2019 level, but decreases to 78.8% in the 8–12 ppm interval and to 37.5% in the above 20 ppm interval. This indicates that ambiguity fixing becomes increasingly sensitive to ionospheric disturbances when I95 exceeds about 8 ppm, particularly under the more active ionospheric conditions encountered in 2024.

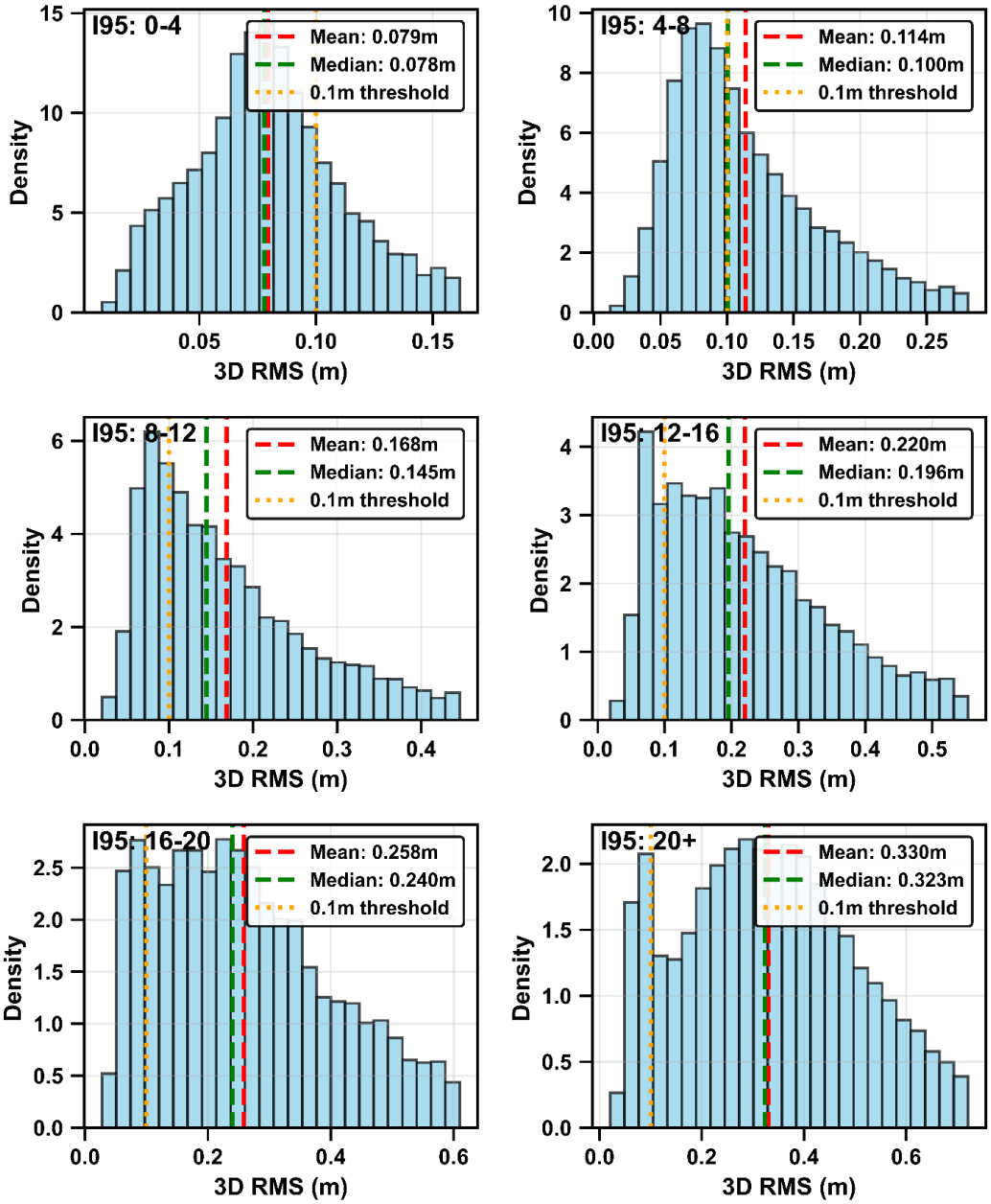


Fig. 7 Distribution of 3D-RMS error positioning errors in 2024 for different I95 intervals. Dashed vertical lines denote the mean and median values, and dotted lines indicate the 0.1 m reference threshold.

Fig. 7 is restricted to the 2024 dataset, which covers a wider range of I95 values and thus provides better sampling of disturbed ionospheric conditions. A 3D-RMS value of 0.1 m is adopted as a practical reference separating centimeter- and decimeter-level positioning performance. For I95 values below 4 ppm, most errors remain below or close to this level, with a mean value of 0.079 m. With increasing I95, the distributions shift toward larger errors and become more dispersed. The mean error reaches 0.330 m for I95 values above 20 ppm, while exceedances of 0.1 m become increasingly frequent from the 8–12 ppm interval onward. Elevated I95 is associated with both a higher

characteristic error level and larger dispersion of the positioning solutions.

The concurrent reduction in ambiguity-fixing rate and broadening of the 3D-RMS distribution are consistent with increased residual ionospheric and spatial-interpolation errors under disturbed conditions. At low I95, these residuals contribute only marginally to the user error budget. At elevated I95, however, enhanced spatial variability reduces the representativeness of the interpolated corrections and increases the likelihood of degraded positioning performance. The interval-based analysis identifies the I95 ranges over which this degradation becomes apparent, but does not reveal whether the response is uniform throughout the error.

Quantile regression is thus employed to characterize the conditional error response. The selected quantiles, $\tau = 0.05$, 0.33, 0.50, 0.67, and 0.95, represent the lower tail, lower-middle range, median, upper-middle range, and upper tail of the 3D-RMS distribution, respectively. This selection enables the sensitivity of both typical and extreme positioning errors to I95 to be assessed. The fitted relationships for 2019 and 2024 are shown in Fig. 8. For each quantile, the slope β denotes the change in the corresponding conditional quantile of 3D-RMS per unit increase in I95.

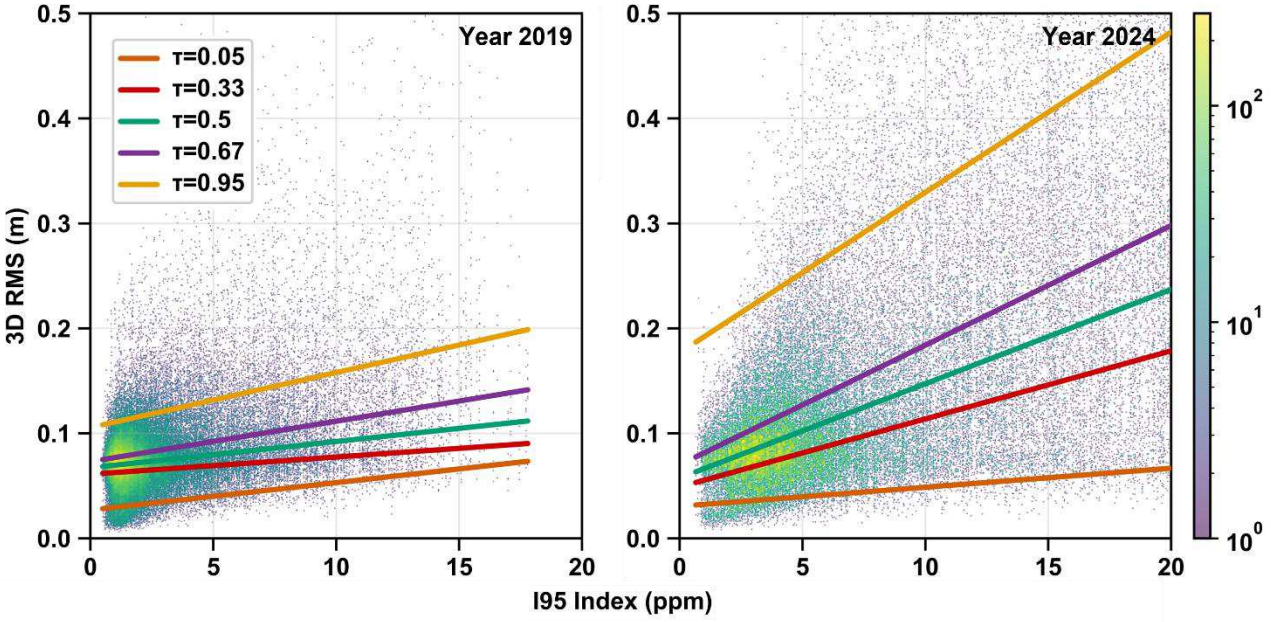


Fig. 8 Quantile regression of 3D-RMS error positioning error as a function of I95 for 2019 and 2024.

All fitted slopes in 2024 are positive and increase from $\beta = 0.0018$ at $\tau = 0.05$ to $\beta = 0.0153$ at $\tau = 0.95$. The upper-tail slope is approximately 8.5 times the lower-tail slope, indicating that the dependence on I95 is concentrated in the upper part of the conditional error distribution rather than represented by a uniform shift of all error levels. Positive slopes are also obtained for 2019, although their increase toward the upper tail is less pronounced. At $\tau = 0.95$, the 2019 slope amounts to 0.0052, corresponding to about one third of the 2024 value. At $\tau = 0.05$, by contrast, the 2019 slope of 0.0020 slightly exceeds the corresponding 2024 value of 0.0018. The enhanced response in 2024 is confined

mainly to the middle and upper quantiles. This behavior is consistent with the broader range and more frequent occurrence of disturbed conditions in 2024, although the year-to-year comparison alone does not establish a causal effect of solar activity.

Table 2 Quantile-regression slopes relating 3D-RMS error to I95 in 2019 and 2024.

τ	2019		2024		Ratio $\beta_{2024}/\beta_{2019}$
	β	95% CI	β	95% CI	
0.05	0.002009	(0.001909, 0.002109)	0.001811	(0.001724, 0.001878)	0.90
0.33	0.001644	(0.001548, 0.001747)	0.006484	(0.006359, 0.006621)	3.94
0.5	0.002505	(0.002376, 0.002621)	0.008979	(0.008846, 0.009102)	3.58
0.67	0.003841	(0.003726, 0.003935)	0.011391	(0.011255, 0.011510)	2.97
0.95	0.005239	(0.005008, 0.005463)	0.015271	(0.014954, 0.015634)	2.91

The numerical results in Table 2 confirm a positive association between I95 and positioning error at all considered quantiles. The confidence intervals remain above zero in both years. For the middle and upper quantiles, the intervals are clearly separated, indicating a substantially stronger I95 dependence in 2024. At τ=0.95, the 2024 slope is about three times the 2019 value. At τ = 0.05, however, the ordering is reversed, with the 2024 confidence interval lying below that of 2019. A formal comparison of the regression coefficients would be required to establish the statistical significance of the interannual slope differences at each quantile. The interval-based and quantile-regression results demonstrate that I95 characterizes both ambiguity-resolution reliability and the susceptibility of NRTK solutions to large positioning errors. These results provide the basis for the empirical regional performance intervals derived in the following subsection.

Empirical I95-based regional risk classification

To derive operationally interpretable I95 intervals, two complementary user-domain indicators are analyzed jointly: the exceedance probability of 3D-RMS > 10 cm, which characterizes the frequency of degraded solutions, and the cumulative positioning error normalized by baseline length, which reflects the magnitude and dispersion of the error response.

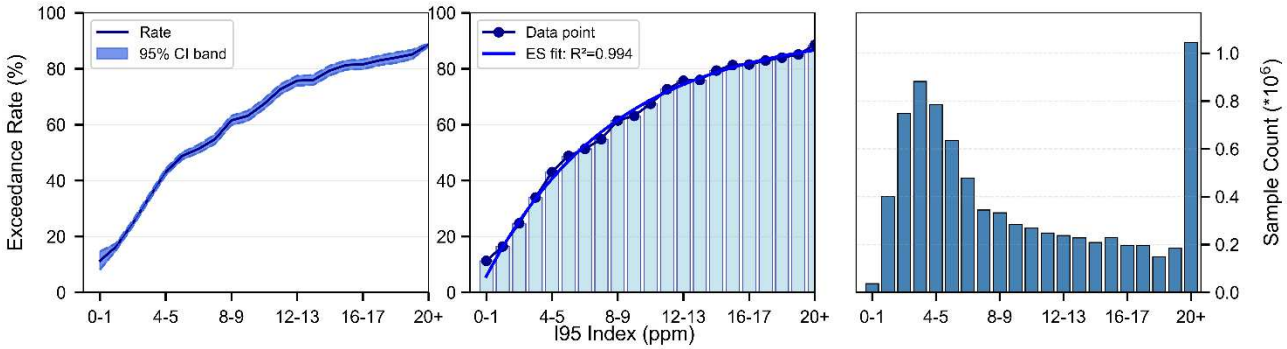


Fig. 9 Exceedance probability of 3D-RMS error above 10 cm as a function of I95 in 2024. The left panel shows the binned exceedance rate with 95% confidence intervals, the middle panel shows the fitted exponential saturation model, and the right panel gives the sample count in each I95 bin.

Fig. 9 shows the probability of 3D-RMS exceeding 10 cm as a function of I95 for 2024. The exceedance probability increases from 11.32% in the 0–1 ppm bin to 88.52% for I95 values above 20 ppm. The increase is most pronounced at low and moderate I95 levels and gradually weakens toward higher values, indicating a saturation-type response that is adequately represented by the fitted exponential model. The confidence intervals remain narrow over most of the I95 range, owning to the large number of epoch-wise samples available in each bin. According to the fitted relation, exceedance probabilities of 40%, 60%, and 80% are reached at I95 values of approximately 4.16, 8.28, and 14.83 ppm, respectively. The lower bounds of the corresponding 95% confidence intervals first exceed these probability levels in the 4–5, 8–9, and 15–16 ppm bins.

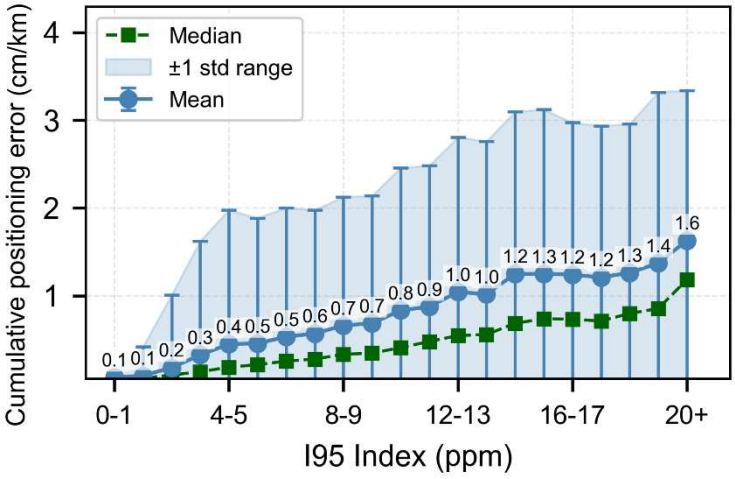


Fig. 10 Cumulative positioning error normalized by baseline length as a function of I95 in 2024. Markers indicate the mean and median values for each I95 bin, and the shaded band denotes the ± 1 standard deviation range.

Fig. 10 shows the baseline-normalized cumulative positioning error for the same I95 intervals. The mean value increases from 0.07 cm/km in the 0–1 ppm interval to 1.56 cm/km for I95 values above 20 ppm, while the median rises from 0.05 to 1.11 cm/km. The dispersion likewise increases, with the standard deviation growing from 0.33 to 1.71 cm/km. Only limited changes are observed below 4 ppm, whereas a more pronounced increase occurs for 4–10 ppm and continues over the 10–16 ppm range. Above 16 ppm, both the magnitude and dispersion of the cumulative error remain high. Increasing I95 is associated not only with a higher probability of exceeding the 10 cm error threshold, but also with a systematic increase in the magnitude and variability of the positioning error.

The boundaries near 4, 10, and 16 ppm are selected from the combined behavior of the two

indicators. The first boundary, near 4 ppm, marks the onset of sustained degradation: the fitted exceedance probability reaches 40% at approximately 4.16 ppm, the lower confidence bound first exceeds 40% in the 4–5 ppm interval, and the cumulative error begins to increase more persistently beyond this range. The second boundary, near 10 ppm, lies within the transition from approximately 60% to 70% exceedance probability and coincides with a further rise in cumulative error. The third boundary, near 16 ppm, marks severe degradation: the fitted exceedance probability approaches 80%, the lower confidence bound exceeds this level in the 15–16 ppm interval, and both the magnitude and dispersion of the cumulative error remain high. Accordingly, the intervals below 4, 4–10, 10–16, and above 16 ppm can be adopted as empirical performance regimes for the Hong Kong network, rather than sharp physical thresholds.

Table 3 Empirical I95 intervals and associated NRTK performance characteristics for the Hong Kong low-latitude network.

Risk Level	**Low**	**Moderate**	**High**	**Extreme**
I95 range (ppm)	< 4	4-10	10-16	> 16
Cumulative error per km (cm/km)	median < 0.2 mean < 0.4	median 0.2–0.5 mean 0.4–0.8	median 0.5–0.8 mean 0.8–1.2	median 0.8–1.2 mean 1.2–1.6
Ambiguity-fixing rate	> 95%	80%–95%	60%–80%	< 60%
Exceedance probability of 3D-RMS > 10 cm	< 40%	40%-70%	70%-80%	> 80%

Table 3 summarizes the four I95 intervals and the associated ambiguity-fixing, exceedance-probability, and cumulative-error characteristics. Since the boundaries are derived from the observed user-domain response, they should be considered as empirical thresholds calibrated for the Hong Kong network.

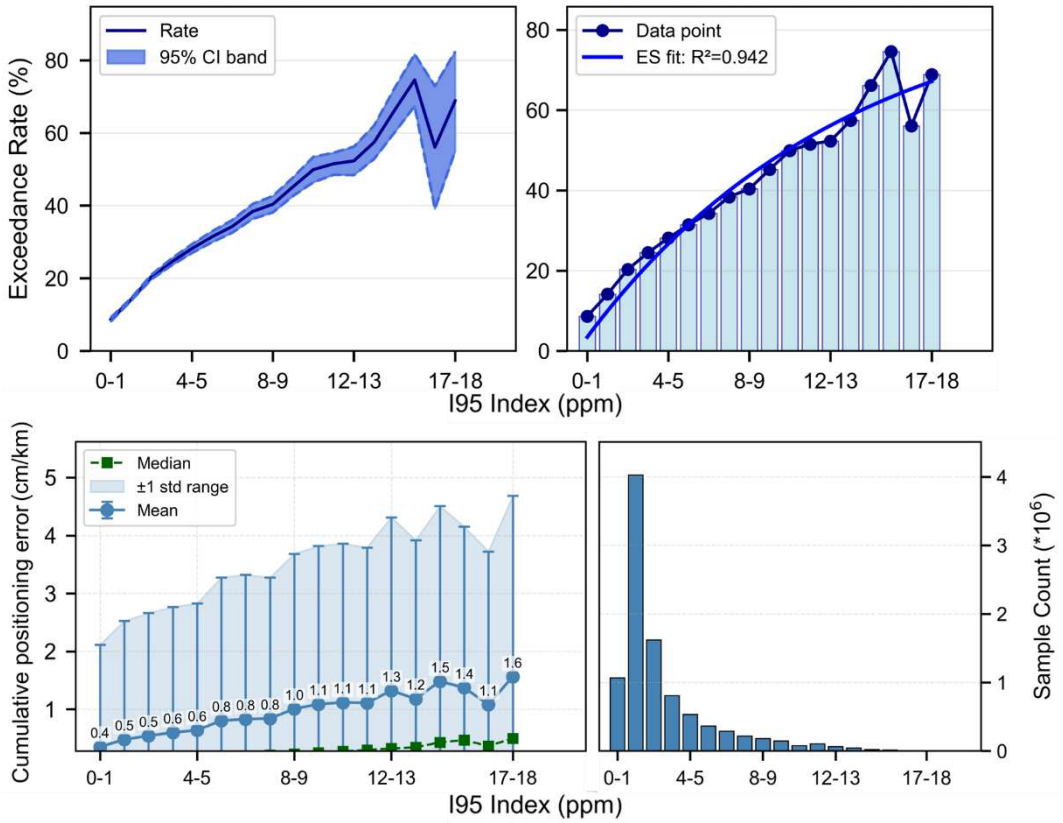


Fig. 11 Cross-year consistency check of the I95-based performance assessment using the 2019 data. The panels show the exceedance probability of 3D-RMS errors above 10 cm, the exponential saturation fit, the cumulative positioning error per kilometer of baseline, and the sample count for each I95 bin.

Fig. 11 provides a cross-year assessment using the 2019 dataset, which represents quieter solar and ionospheric conditions. The exceedance probability increases from 8.62% in the 0–1 ppm interval to 74.60% in the 15–16 ppm interval, while the mean error rises from 0.3871 to 1.42 cm/km. The fitted probability levels of 40%, 50%, 60%, and 70% are reached at approximately 8.32, 10.56, 13.79, and 17.10 ppm, respectively. Compared with 2024, the response is weaker and shifted toward higher I95 values. The general ordering of the performance regimes is preserved. However, the limited high-I95 samples in 2019 provides stronger evidence for the intervals below 16 ppm than for the regime above 16 ppm. This is consistent with the lower occurrence of strongly disturbed intervals during periods of weaker solar activity.

The proposed classification is calibrated for the Hong Kong low-latitude network, but cannot be considered as a general standard for NRTK services. Its applicability to mid- and high-latitude regions, as well as to networks with different station spacings, geometries, observation environments, and processing strategies, remains to be investigated. Nevertheless, the analysis framework can be transferred to other regional networks to derive locally calibrated I95 performance intervals, provided that sufficiently long datasets covering representative ionospheric conditions are available.

Conclusions

This study investigated the use of I95 as a residual-based indicator of NRTK positioning degradation in a low-latitude regional network. Full-year GPS observations from the Hong Kong CORS network in 2019 and 2024 were processed using a leave-one-out VRS strategy. The resulting I95 values were compared with user-side ambiguity fixing, 3D positioning errors, exceedance probabilities, and cumulative positioning errors.

NRTK performance deteriorated systematically with increasing I95. In 2019, I95 remained low for most of the year, ambiguity-fixing rates were generally high, and positioning errors were largely confined to the centimeter level. In 2024, elevated I95 values were associated with lower ambiguity-fixing rates and broader error distributions. The quantile regression results further showed that the dependence on I95 increased toward the upper tail of the positioning error distribution. Residual ionospheric activity therefore affected primarily the occurrence and magnitude of large-error events rather than producing only a shift in the average error level.

Based on the probability of 3D positioning errors exceeding 10 cm and the cumulative positioning error normalized by baseline length, four empirical I95 performance regimes were identified for the Hong Kong network: <4, 4-10, 10-16, and >16 ppm. These intervals characterize conditions ranging from generally stable NRTK performance to substantially reduced ambiguity-fixing reliability and frequent dm-level errors. The analysis of the 2019 data preserved the general ordering of these regimes, although the response was weaker and the number of samples at high I95 values was limited.

The derived intervals are specific to the Hong Kong low-latitude network and should not be interpreted as overall NRTK warning thresholds. Their applicability to other regions requires further verification. Longer observation records and independent regional datasets will be required to assess the robustness and transferability of the proposed classification under a broader range of ionospheric conditions.

Acknowledgments

The authors gratefully acknowledge the Survey and Mapping Office of the Lands Department for providing observations and station coordinates from the Hong Kong Satellite Positioning Reference Station Network. The authors also thank the LGLN in Germany for providing the operational I95 product used to assess the external consistency of the implemented I95 computation.

Funding

This work was funded by the Shandong Key R&D Program (2024YFB3908802), National Natural Science Foundation of China (42404013), Beijing Nova Program (20230484329), Jinan Haiyou Leading Talents Of Industry and Youth Innovation Promotion Association of the Chinese Academy of Sciences.

Authors' contributions

L Z designed the research, developed the software, processed the data and wrote the manuscript. N W and B L proposed the key idea and contributed to manuscript writing. Z L (Z Li) and C W contributed to the interpretation of the ionospheric disturbance analysis and provided critical comments on the manuscript. M S, Z L (Z Liu) and Z W contributed to data checking, result interpretation, and manuscript revision. All authors reviewed and approved the final manuscript.

Data availability

The GNSS observations used in this study were obtained from the Hong Kong Satellite Positioning Reference Station Network (https://www.geodetic.gov.hk/common/data/). The LGLN I95 product was used for the external consistency assessment. The derived datasets are available from the corresponding author upon reasonable request.

References

Chen X, Landau H, Vollath U (2003) New tools for network RTK integrity monitoring. Proceedings of the 16th International Technical Meeting of the Satellite Division of The Institute of Navigation:1355–1360.

Gao W, Zhang Z, Pan S, Liu H, Tao X, Zhao Q (2025) An adaptive NRTK ionospheric regional modeling method integrating baseline neighborhood enhancement and weighted lower-order surface model. Measurement.

Gianniou M, Mitropoulou E (2012) Impact of high ionospheric activity on GPS surveying: Experiences from the Hellenic RTK-network during 2011–12. EUREF Annual Symposium 2012:6–8.

Guerra M, Cesaroni C, Ravanelli M, Spogli L (2024) Travelling ionospheric disturbances detection: a statistical study of detrending techniques, induced period error and near real-time observables. Journal of Space

Weather and Space Climate 14:17.
Li A, Wang N, Hernández-Pajares M, Liu A, Li Z, Rülke A, Krankowski A, Yang H, Ghoddousi-Fard R, Froń A, Zhang Z (2026) RT-FAIRS: Real-Time Factor-Adjusted Ionospheric Residual Statistics Approach for Generating Accuracy Information in Global Ionospheric Maps. Space Weather 24(4):e2025SW004769.
Li Z, Wang N, Hernández-Pajares M, Yuan Y, Krankowski A, Liu A, Zha J, García-Rigo A, Roma-Dollase D, Yang H, Laurichesse D, Blot A (2020) IGS real-time service for global ionospheric total electron content modeling. Journal of Geodesy 94(3):32.
Li Z, Zhong J, Wang N, Hao Y, Wan X, Jakowski N, Hoque MM, Liu A, Li Z, Liu R, Nykiel G (2025) Ionospheric gradient estimation using ground-based GEO observations for monitoring multi-scale ionospheric dynamics. Satellite Navigation 6(1):30.
Liu T, Chen W, Mi X, Chen X, Yang Y, Ding J, Liu T, Wang Y, Weng D (2026) Ionospheric nonlinear interpolation model for Mid- and Low-latitude network RTK during solar maxima. GPS Solutions 30:7. https://doi.org/10.1007/s10291-025-01976-9
Lyu Z, Wang N, Li Z, Wang Z, Wang L, Liu B (2025) Characterization of BDS-3 precise orbit, clock and multi-frequency phase bias products for integrity monitoring. Advances in Space Research 77(2):2074–2093.
Naciri N, Bisnath S (2023) RTK-quality positioning with global precise point positioning corrections. NAVIGATION: Journal of the Institute of Navigation 70(3):navi.575. https://doi.org/10.33012/navi.575
Niell AE (1996) Global mapping functions for the atmosphere delay at radio wavelengths. J Geophys Res Solid Earth 101(B2):3227–3246. doi:10.1029/95JB03048.
Nykiel G, Cahuasquí JA, Hoque MM, Jakowski N (2024) Relationship between GIX, SIDX, and ROTI ionospheric indices and GNSS precise positioning results under geomagnetic storms. GPS Solutions 28(2):69.
Paziewski J (2016) Study on Desirable Ionospheric Corrections Accuracy for Network-RTK Positioning and Its Impact on Time-to-Fix and Probability of Successful Single-Epoch Ambiguity Resolution. Advances in Space Research 57(4):1098–1111.
Próchniewicz D, Szpunar R, Walo J (2017) A new study of describing the reliability of GNSS Network RTK positioning with the use of quality indicators. Measurement Science and Technology 28(1):015012. https://doi.org/10.1088/1361-6501/28/1.015012
Teunissen PJG (1995) The least-squares ambiguity decorrelation adjustment: a method for fast GPS integer ambiguity estimation. J Geod 70(1):65-82
Teunissen PJG, Verhagen S (2004) On the foundation of the popular ratio test for GNSS ambiguity resolution. In: Proceedings of the 17th International Technical Meeting of the Satellite Division of the Institute of Navigation (ION GNSS 2004), Long Beach, CA, 21-24 September 2004, pp 2529-2540
Wang N, Li Y, Li Z, Liu A, Liu B (2026) Determination of multi-GNSS differential code biases with satellite antenna phase center corrections. GPS Solutions 30(1):22.
Wanninger L (1999) The Performance of Virtual Reference Stations in Active Geodetic GPS-networks under Solar Maximum Conditions. Proceedings of the 12th International Technical Meeting of The Institute of Navigation:1419–1428.
Wanninger L (2004) Ionospheric disturbance indices for RTK and network RTK positioning. Proceedings of the 17th International Technical Meeting of The Institute of Navigation:2849–2854.
Weaver BJ (2023) Kinematic Precise Point Positioning Algorithm Development and Improvements using External Atmospheric Information. PhD thesis, University of Nottingham.
Zhang W, Zhang J, Zuo X, Li H, Pan G, Wang J (2025) New data processing methods for network RTK positioning: improving ionospheric uncertainty management during ionospheric scintillations. GPS Solutions 29(2):72.
Zhang Z, Wang N, Liu A, Li Z, Li A, Wang L, Zhang Y (2025) Assessing 1-second ROTI for ionospheric perturbation monitoring using real-time multi-GNSS data in China. Space Weather 23(2):e2024SW004187.